Molecular Dynamics Simulation of Uniaxial Deformation of Glassy Amorphous Atactic Polystyrene

4 AUTHORS, INCLUDING:

Nikolay K. Balabaev
Russian Academy of Sciences

133 PUBLICATIONS   948 CITATIONS

SEE PROFILE

Mikhail Abramovich Mazo
Semenov Institute of Chemical Physics

50 PUBLICATIONS   334 CITATIONS

SEE PROFILE

Molecular Dynamics Simulation of Uniaxial Deformation of Glassy Amorphous Atactic Polystyrene

Alexey V. Lyulin,*,† Nikolaj K. Balabaev,‡ Mikhail A. Mazo,§ and M. A. J. Michels†

Group Polymer Physics, Eindhoven Polymer Laboratories and Dutch Polymer Institute, Technische Universiteit Eindhoven, P.O. Box 513, 5600 MB Eindhoven, The Netherlands; Institute of Mathematical Problems of Biology, Pushchino, 142290 Russia; and Institute of Chemical Physics, Moscow 117977, Russia

ABSTRACT: Molecular dynamics computer simulations have been carried out of a chemically realistic many-chain nonentangled model of glassy atactic polystyrene under the influence of uniaxial mechanical deformation. Both the initial elastic and the postyield (up to 100% of the deformation) behavior have been simulated. The Poisson ratio, the Young modulus, and the temperature dependence of the yield peak are well reproduced. The simulated strain-hardening modulus is in quantitative agreement with existing experiments. The deformationally induced anisotropy in the global and local segmental orientation is accompanied by an anisotropy of the local translational mobility: the mean-square translational displacement of the individual segments in the direction of the deformation is drastically increased just beyond the yield point as compared to the isotropic sample. The mechanical deformation of a quenched sample leads to an almost complete erasure of the aging history.

1. Introduction

Amorphous polymers are practically relevant due to the unique properties which control their ductility, toughness, and impact resistance. Studies on the mechanical behavior of amorphous polymers have a long history, received considerable attention of the polymer research community, but still suffer from empiricism. From tensile testing experiments[1] it is generally concluded that a polymer like atactic polystyrene (PS) is brittle and a polymer like bisphenol A polycarbonate (PC) is ductile, but the underlying mechanisms of this difference between these two amorphous polymers remain unclear. In addition, the picture is more complex than this since the macroscopic deformability of PC disappears if a specimen is notched and tested under impact conditions. On the other hand, it is found that by mechanical treatment PS and PC can both macroscopically become very ductile and can be deformed by shear yielding.[2,3] However, the relaxation back to the original state is orders of magnitude faster for PS than PC.

This long-standing but still puzzling subject of great practical relevance has in the past few years seen a number of important new developments which help to understand the relation between chemical nature and mechanical behavior, in particular by fundamental, physics-based methods. First of all, it has proved possible[4] to measure the intrinsic large-deformation stress−strain behavior at a microscopic scale, with the surprising result that e.g. PS is at that level far more ductile than PC. In fact, there exists an excellent correlation between the microscopically measured maximum extension ratio and the theoretical maximum extension ratio of a single strand in the polymer entanglement network. A second major step was to relate this microscopic constitutive behavior to the observed experimental one at a macroscopic scale and to understand the reversal in ductility between PS and PC. Smit, Brekelmans, and Meijer[5] were the first to do multilevel micro−macromodeling, with the microscopic elasto−viscoplastic constitutive equation as an input, with large-strain micro−macrohomogenization of heterogeneous domains and with a subsequent finite-element representation of the microstructure. They were able to predict the global mechanical behavior of filled amorphous polymers under different loading conditions from the microstructure and microscopic properties. An important new insight is that what matters is not so much the absolute value of the yield stress, but more the balance between the postyield stress dip and the strain hardening.[5] But in this approach both the origin and variety of the microscopic stress−strain behavior and the difference in relaxational properties between different amorphous polymers remain an open problem.

Concerning the relation with the molecular behavior, it has recently become clear that both crazing and yielding of amorphous polymers are intimately linked to the collective segmental dynamics of individual or neighboring chains.[6] Recent time-of-flight neutron-scattering measurements and neutron spin-echo experiments also serve as experimental evidence that this collective dynamics in the amorphous phase is the overriding phenomenon. Jérôme[7] showed that, by taking advantage of confinement effects in thin nonpolymer films, the molecular dynamics below the glass transition can be probed experimentally and the collective character of molecular motions can be revealed. The use of intuitive insight into the chain flexibility and dynamics for molecular design and synthesis of tough glassy polymers has recently been demonstrated spectacularly by Yee et al.[6]

One of the first detailed dynamic computer simulations of an amorphous polyethylene-like polymer under tension has been performed by Brown and Clarke.[8] They

† Technische Universiteit Eindhoven.
‡ Institute of Mathematical Problems of Biology.
§ Institute of Chemical Physics.
* To whom correspondence should be addressed. E-mail: a.v.lyulin@tue.nl.

considered a uniaxial deformation experiment with different tension rates for a single linear polymer chain of $N_p = 1000$ sites that forms a dense amorphous state. A loose-coupling constant-pressure molecular dynamics (MD) simulation has been carried out for times up to 1 ns. The simulated elastic deformation, yield, and plastic flow at low temperatures show strong similarity with laboratory results obtained on time scales orders of magnitude longer. Lattice and off-lattice Monte Carlo simulations of deformed polymer melts have been performed by Hölzl et al.[9] and Chui and Boyce,[10] respectively. Hölzl et al.[9] show that the simulated stress−strain relations qualitatively agree with experimental findings. At temperatures near the glass transition the simulated polymer sample shrinks laterally during the deformation, with a Poisson ratio of 0.15. At temperatures below T_g, voids are produced and the chains are extremely stretched. An amorphous polymer network under large-strain deformation has been studied by Chui and Boyce[10] by means of the Monte Carlo simulations for a three-dimensional polybead model. A stepwise affine deformation was applied to the model via a series of strain increments followed by a number of Metropolis minimization cycles. After yield, both strain-softening and strain-hardening phenomena have been reproduced.

The increase of the local chain mobility under uniaxial deformation in the amorphous region of a semicrystalline polymer (nylon-6) has been examined experimentally by Loo, Cohen, and Gleason[11] using solid-state deuterium NMR. The uniaxial deformation enhances the number of deuterated groups with high mobility. This enhanced mobility decayed rapidly once deformation was stopped. Capaldi, Boyce, and Rutledge[12] recently performed MD simulations of a model glassy amorphous polyethylene in compression at a strain rate of 10^{10} s^{-1} at $T = 200$ K $< T_g = 280$ K. The simulated results reproduce the experimentally observed phenomenon of the stress-induced mobility (despite the obvious difference in the time scales probed by the MD simulations and by the NMR experiment) and relate it to the increase of the dihedral angle transition rate. This transition rate drops when active deformation ceases, also in agreement with the NMR results.[11]

Brownian dynamics simulations of Neelov, Darinskii, and Clarke[13] for a toy model single polymer chain in an external field of dipolar symmetry also reveal the significant change of the local segmental mobility under deformation. It was shown that the extension of the polymer chain proceeds in two stages. During the first stage the extension involves the redistribution of the coiled and extended rotational isomers along the chain, the overall conformational composition being retained. The extension during the second stage involves the transition of the coiled isomers to the extended isomers. It was shown that near the extended conformations ($t \leftrightarrow g^{+-}$ transitions), the local conformational mobility increases, whereas it decreases for the coiled conformation ($g^{+-} \leftrightarrow g^{-+}$ transitions).

MD simulation of the anisotropic mechanical properties of an oriented amorphous poly(ethylene terephthalate), PET, has been reported by Zhou et al.[14] up to a draw ratio $\lambda = 3.9$. Eight chains of PET consisting of only 10 monomers each were first randomly packed into an orthorhombic box at $T = 300$ K. Then they were uniformly deformed by a constant NVT MD such that they end up as a cube. The change in cell dimension

every 200 fs was 0.35%. For the amorphous cells, with the initial length of $c = 6.4$ Å, this deformation velocity is about 0.1 Å/ps. The observed rapid development of the benzene rings orientation with deformation is in good agreement with the results of polarized infrared spectroscopy, but it should be noticed that the simulation cells develop orientation more rapidly than is seen in the experiment. The development of the main-chain bonds orientation in the direction of stretching was observed by Ogura and Yamamoto[15] in the MD simulation of a polymethylene melt.

In the present paper MD computer simulations are reported for a chemically detailed model melt of atactic PS in the glassy state under the influence of uniaxial deformation. Both the linear elastic regime and the nonlinear regime of large deformation, up to 100%, have been simulated. The main attention has been paid to the investigation of conformational and local dynamical properties of the polymer glass in an anisotropic deformed state. The motion of the bulky side groups (phenyl rings) is taken into account explicitly. We focus on the changes in translational mobility of the main-chain and the side-group segments and the orientation of the chain bonds. To our knowledge, it is the first effort to use the atomistic simulations of such degree of detail in order to study the bulk mechanical, conformational, and segmental dynamical properties of a model amorphous polymer under uniaxial deformation. The model and the simulation algorithm are described in section 2. In section 3 the bulk mechanical properties, the onset of the yield behavior, and orientational characteristics of the main-chain segments and side phenyl rings are discussed. Section 4 shows the results for local translational mobility of the chain segments. The simulated quenching is discussed in section 5. Some conclusions are summarized in section 6.

2. Model and Simulation Algorithm

The united-atom model of PS described in detail in our previous study[16,17] is explored also in the present paper. The simulation has been performed for two systems: eight chains of $N_p = 80$ monomers each (molecular weight ~ 8300) and four chains of $N_p = 160$ monomers (molecular weight $\sim 17\,000$). In the second case the chain length is close to the entanglement length for this polymer. The stereochemic configurations of the aromatic groups were generated at random so that the ratio of number of *meso* to number of *racemic* dyads was near unity. For the detailed forms of the potential contributions and the values of the potential constants we refer to ref 16.

The leapfrog variant of the velocity Verlet algorithm[18] has been used to integrate the Newtonian equations of motion. Equilibration has been performed by the Berendsen NPT molecular dynamics algorithm[19] for up to 20 ns, with time constants $\tau_T = 0.5$ ps and $\tau_P = 1$ ps and with an integration time step $\Delta t = 4$ fs, at (isotropic) atmospheric pressure and high temperature, $T = 650$ K, corresponding to the high-mobility melt. The system was next cooled with a constant cooling rate of 0.05 K/ps to different lower temperatures, from 480 to 240 K, covering the temperature region in the vicinity of $T_g \sim 370$ K. To simulate the effect of rapid quenching, the 4 $\times$ 160 system was cooled from $T = 600$ K to $T = 260$ K within about 2 ps, giving an effective cooling rate of 170 K/ps, more than 3 orders of magnitude faster than the regular cooling rate implemented in the present study.

Uniaxial deformation along three Cartesian axes was applied independently to five independent sets of relaxed isotropic PS samples at various temperatures. Final results have been averaged over all five sets and three directions of deformation. Then nominal strain parallel to the direction of deformation has been measured as

$$\gamma_L = \frac{L - L_0}{L_0} \times 100\% \qquad (1)$$

where L is the instant length of the simulation box parallel to the direction of the applied tension and L_0 denotes the equilibrium value of this length prior to the application of tension. From the cross-sectional area A perpendicular to the direction of the deformation, an effective width can be defined as $W = A^{1/2}$. The effect of the applied stress can be resolved in the parallel nominal strain γ_L and the perpendicular nominal strain

$$\gamma_W = \frac{W - W_0}{W_0} \times 100\% \qquad (2)$$

As in eq 1, the subscript denotes the equilibrium value averaged over all relaxed samples at the prescribed temperature. Uniaxial deformation was also applied along three Cartesian axes to two independent sets of quenched isotropic PS samples at $T = 260$ K.

Most of the production runs have been obtained with the constant deformation velocity of $\dot{\gamma} = 0.005$ Å/ps, which is significantly slower than the simulation efforts reported so far in the literature.[8,14,15] Nevertheless, with the initial size of the box $L_0 \sim 50$ Å, the relative deformation rate is very large, 10^8 s^{-1}. To study the effect of the deformation velocity, some runs have been performed at different values of $\dot{\gamma}$, in the range from 0.0005 to 0.005 Å/ps. A Berendsen barostat[19] and the collisional thermostat[20] were used to keep the system at prescribed temperatures and pressures. In all production runs the integration time step was fixed to $\Delta t = 4$ fs; the length of a single run was about 10 ns, which allowed us to reach deformations up to $\gamma_L \sim 100\%$.

3. Simulated Mechanical and Conformational Properties

3.1. Stress−Strain Relation and Mechanical Properties. Our deformation experiments were generally continued until the sample had extended by about 100% of its original length. At temperatures below T_g this deformation leads to stretching of the chains accompanied by some orientation of the chain segments, which will be discussed later. At a low temperature, $T \ll T_g$, and high deformation ratio some cavities and finally a crack are formed. The formation and rapid growth of the cavities were already observed during some simulations of the rupture of adhesive bonds.[21] We should stress here that the simulation of crack formation is far beyond the scope of the present study.

The tension in the system is equal to $-P_{\alpha\alpha}$, where **P** is the stress tensor and α denotes the Cartesian coordinate in the direction of the deformation. In Figure 1 the calculated tension is plotted against the percentage deformation, γ_L, for few temperatures in the vicinity of T_g.

The initial elastic regime (Figure 1b) is clearly seen for extensions up to 3% and is followed by the yield point
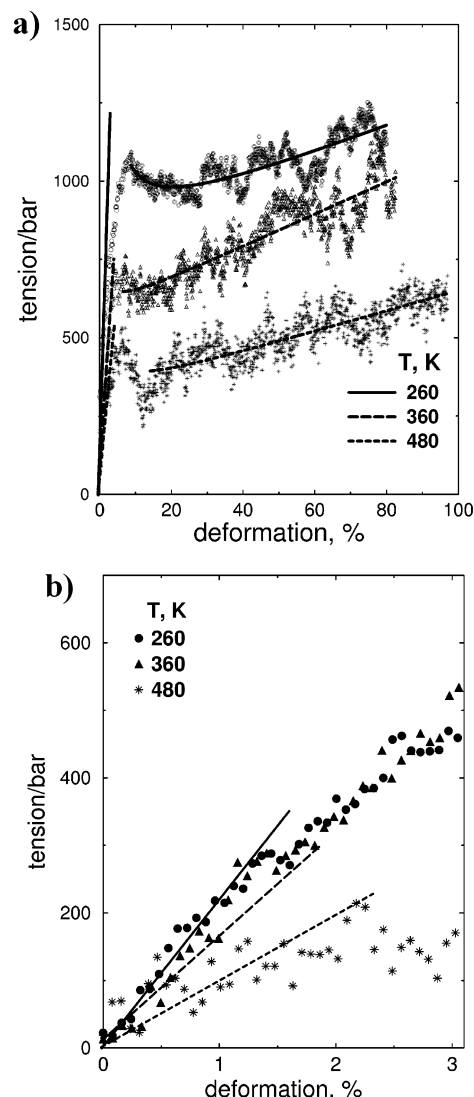

Figure 1. Measured tension $(-P_{\alpha\alpha})$ as a function of the percentage deformation for a 4×160 system for tension applied at $\dot{\gamma} = 0.005$ Å/ps. The data at each temperature represent the average behavior over five independent samples and three independent directions of the deformation. The figure shows the full stress−strain curves (a) and their initial elastic regimes of small deformation (b). Straight lines in (a) are drawn as a guide to the eye.

at $\gamma_L \sim 3-4\%$, the strain-softening regime for γ_L up to 15%, and some strain hardening for higher deformations.

The density response of the system at different temperatures was examined at the deformation velocity $\dot{\gamma} = 0.005$ Å/ps for a 4×160 system. At high temperature $T > T_g$, the deformation process is mainly viscous, and there is almost no noticeable change in the density during deformation (Figure 2). At low temperature $T < T_g$, there exists some dilation effect during the initial stage of the deformation, $\gamma_L < 10\%$. After the yield point the density is almost constant in a broad temperature range. The value of this constant slightly increases with decreasing the deformation velocity. The detailed study of the impact of the deformation velocity on the reported properties should be a subject of our future investigation.

At very low temperatures, $T < 260$ K, and rather high deformations, $\gamma_L > 40\%$, the density starts to decrease, and the crack is formed. The initial decrease in density
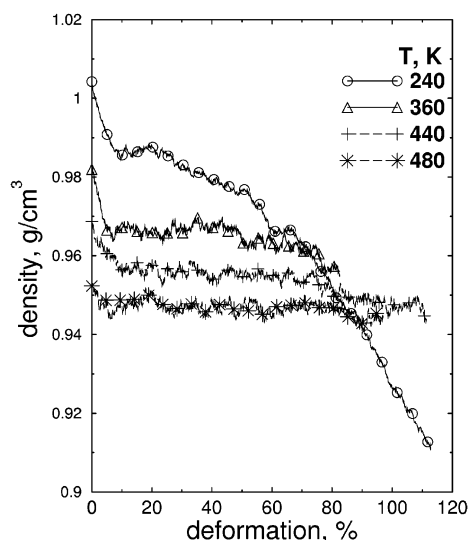
Figure 2. Deformation dependence of the density during the extension experiment at different temperatures and with deformation velocity $\dot{\gamma} = 0.005$ Å/ps for a 4×160 system. At very low temperature after some plateau the density rapidly decreases due to crack formation in the sample.

under deformation is consistent with the calculated value of the Poisson ratio

$$\mu = -\lim_{\gamma_L \to 0} \frac{\gamma_W}{\gamma_L} \qquad (3)$$

which gives a value of $\mu = 0.33 \pm 0.02$ at the lowest simulated temperature, $T = 240$ K (Figure 3a), close to the experimental estimates[22] of $\mu = 0.32-0.33$.

From the slope of the initial parts (up to $\gamma_L = 3\%$) of the stress−strain curves the Young modulus, which quantifies the uniaxial mechanical response of a material in the small-strain regime, is calculated. The value of the Young modulus at low temperatures is about 3 GPa (Figure 3b), which is very close to the experimental value of $\sim 3.2-3.4$ GPa. The Young modulus decays with temperature with the rate of 9 ± 2 MPa/K, which is of the same order as the experimental value (~ 5 MPa/K), and falls to rather small values at high temperature, $T > 420$ K, well above the glass transition.

At $\gamma_L > 3\%$ the simulated polymer glass starts to yield. The yield stress τ can be expressed in terms of strain rate as[22]

$$\tau = \frac{\Delta H}{v} + \frac{RT}{v} \ln \frac{2\dot{\gamma}}{\dot{\gamma}_0} \qquad (4)$$

where ΔH is the activation energy, $\dot{\gamma}$ is the deformation rate, and v is the activation volume, which is considered to represent the volume of the polymer segment which has to move in order for plastic deformation to start. $\dot{\gamma}_0$ is some constant preexponential factor in the Eyring-type theory of nonlinear viscoelastic behavior.[22] The temperature dependence of the yield stress τ is indeed close to linear at temperatures $T < T_g$ (Figure 4), with a slope of -3.6 bar/K. The value of $\Delta H/v$ in eq 4 is obtained by extrapolation of the yield−stress results to zero temperature. Then, solving eq 4 for different values of the deformation rate used at some fixed temperature, the value of the activation volume $v \sim 360 \pm 30$ Å^3 and the activation energy $\Delta H \sim 45 \pm 5$ kJ/mol are obtained. In other words, the characteristic length of the "kinetic"
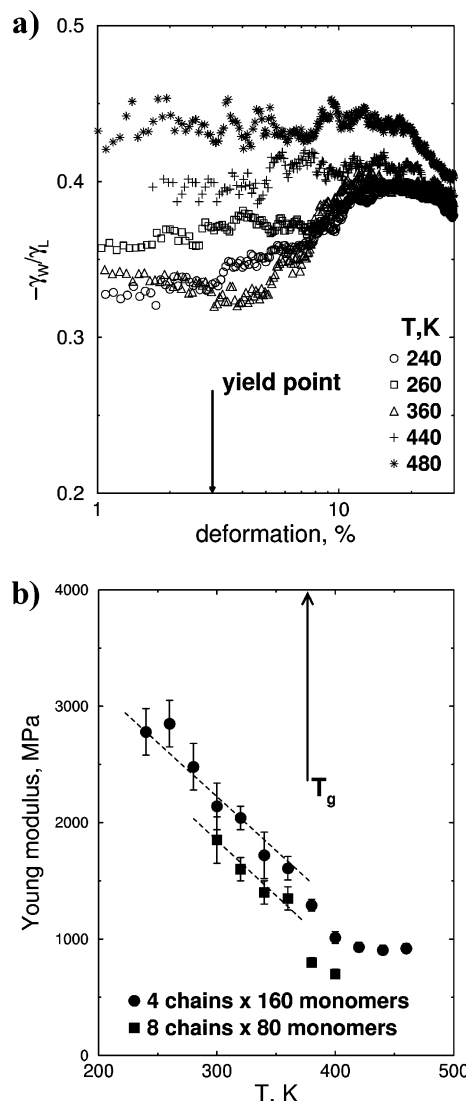

Figure 3. (a) Deformation dependence of the ratio of the extensional and contractile strains for a 4×160 system at different temperatures. At infinitely small deformation this serves as an estimate for the Poisson ratio. (b) Temperature dependence of the Young modulus obtained from small-strain ($<3\%$) behavior for 8×80 and 4×160 systems. Dashed lines represent linear fits to the data. $\dot{\gamma} = 0.005$ Å/ps.

element which starts to flow is about 7 Å, which is 5 times larger than the length of the C−C bond. The experimentally measured[23] strain−rate dependence of the yield peak at different temperatures reveals contributions from at least two different relaxation processes: the main α-relaxation at high temperature (above T_g) and a sub-T_g β-process which starts to contribute to the yield stress at low T. The most important result of this additional contribution is the much faster increase of the yield stress with strain rate and, correspondingly, a faster decrease in the activation volume. In ref 24 the results of mechanical testing experiments on atactic PS (PS N5000, $M_w \sim 300\,000$) have been fitted, giving the value of $v \sim 1800$ Å^3 (and a length of the corresponding "flowing" segment of about 12 Å) for the sub-T_g β-process. The smaller value of the activation volume produced in the present computer simulation could possibly be connected with even faster sub-T_g relaxation processes (γ, δ) contributing to the stress. Such processes could be, in principle, observed experimentally at very low temperatures.
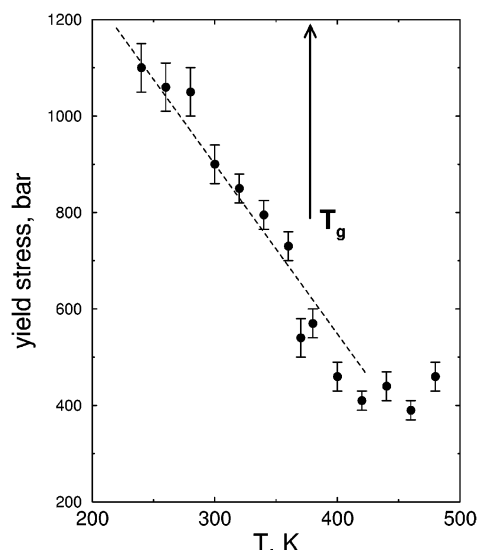
Figure 4. Measured yield stress as a function of temperature for a 4 × 160 system at $\dot{\gamma} = 0.005$ Å/ps. The dashed line represents a linear fit according to eq 4.

After the yield point some strain softening followed by the strain hardening is clearly seen at each simulated temperature, as depicted in Figure 1a. The strain-hardening modulus G_R is usually defined[1] as the slope of the curve at large strains (deformation above 15% in the present simulations) of the true stress σ vs $\lambda^2 - \lambda^{-1}$ (neo-Hookean behavior), $\sigma = G_R(\lambda^2 - \lambda^{-1})$, where $\lambda = L/L_0$. The present simulation data at $T = 260$ K give the value of $G_R = 15$ MPa. Although statistical noise does not allow to make definite conclusions about the temperature dependence of the strain-hardening modulus, its average value $G_R = 13 \pm 3$ MPa (over the range of temperatures from $T = 260$ K to $T = 480$ K) is, nevertheless, in excellent agreement with the experimental result of Van Melick et al.,[1] $G_R = 13$ MPa, produced by the uniaxial compression measurement at $T = 300$ K.

3.2. Orientation of the Chemical Bonds under Deformation. Under uniaxial deformation the polymer chains are strongly stretched and oriented in the direction of the applied tension (Figure 5a,b). Qualitatively, the global orientational anisotropy can be characterized by the projections of the unit vector

$$\mathbf{e} = \frac{\mathbf{h}}{|\mathbf{h}|} \tag{5}$$

where $\mathbf{h} = \mathbf{r_N} - \mathbf{r_1}$ is the end-to-end vector. Figure 6a shows that in the linear regime, i.e., up to ~3% deformation, the polymer coil remains isotropic, with the mean-square parallel and transversal projections of the vector $\mathbf{e}$ equal to $1/3$. The mean-square parallel projection starts to increase drastically beyond the yield point and reaches the value of ~0.65 at γ_L ~100%. Obviously, at the same time the orientation of the polymer coil in the direction perpendicular to the applied tension decreases with deformation.

The global orientation of polymer chains under stretching takes place together with the local ordering of the segments. The orientation of three different unit vectors (see Figure 5a) have been studied: the unit vector $\mathbf{m}$, along the monomer vector in the backbone; the unit vector $\mathbf{s}$, along the vector joining the phenyl group to the backbone; and the unit vector $\mathbf{n}$, along the normal to the plane of the phenyl ring. The deformation dependence of the mean-square parallel projections of the monomer vectors $\mathbf{m}$ in the backbone is shown in Figure 6b, where the pronounced anisotropy of the orientation is seen in the nonlinear regime. The vectors $\mathbf{s}$, joining the phenyl group to the backbone, intend to orient perpendicular to the direction of tension and perpendicular to the monomer vectors $\mathbf{m}$; the value of the average scalar product $\langle \mathbf{s \cdot m} \rangle$ is about zero over the whole range of deformations.

Both the global and local orientation and the stretching of the backbone are accompanied by orientation of the planes of the side phenyl groups. Again, in the linear regime the phenyl planes orient randomly. After the yield point they orient preferably perpendicular to the direction of the macroscopic deformation (i.e., with the vector $\mathbf{n}$ normal to the plane of the ring oriented in the direction of the deformation). The orientation of the phenyl ring planes is completely coupled to the orienta-
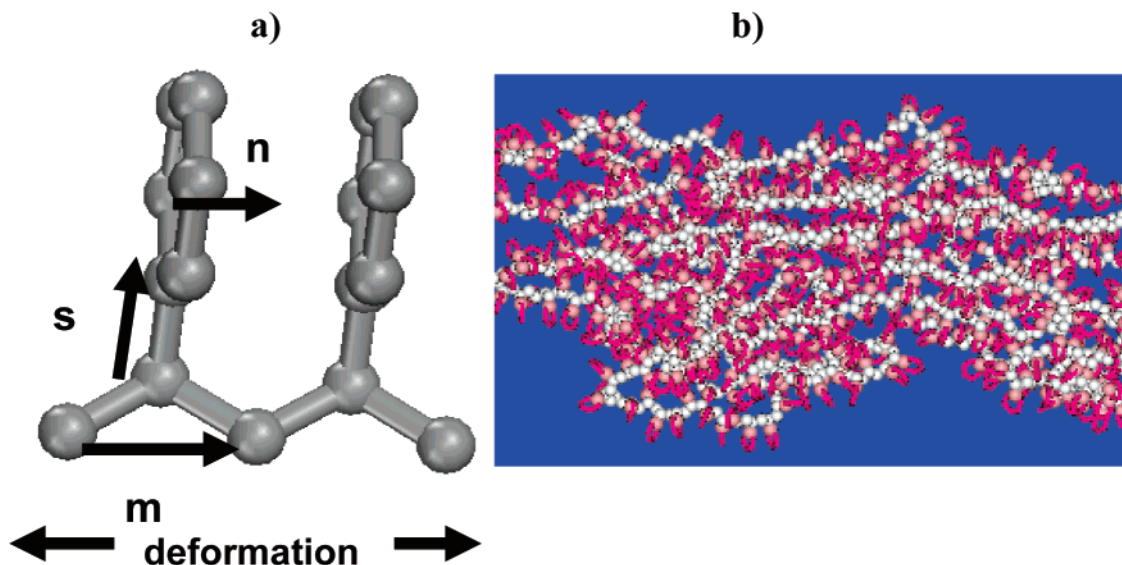

Figure 5. (a) Definition of the three unit vectors used to describe the local orientation of the chain segment: $\mathbf{m}$, for a monomer unit; $\mathbf{s}$, for a side group; $\mathbf{n}$, for a phenyl ring plane. (b) Snapshot of a 4 × 160 system deformed at $\dot{\gamma} = 0.005$ Å/ps. $T = 240$ K, $\gamma_L = 125\%$. The individual chains are highly stretched and oriented in the direction of the applied tension.
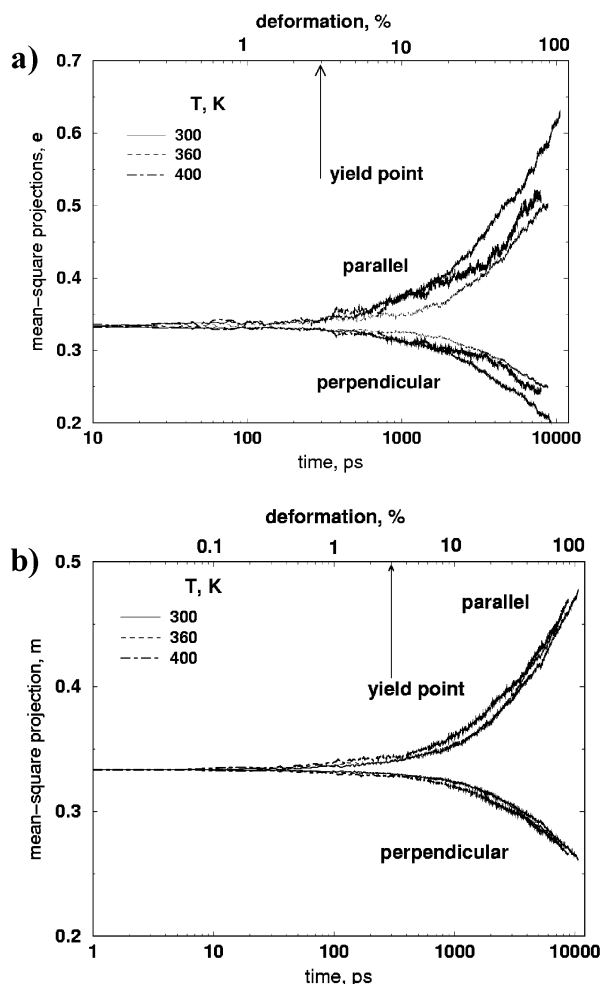
Figure 6. (a) Mean-square projections of the unit vector **e** along the end-to-end distance, parallel and perpendicular to the direction of the deformation. (b) Mean-square projections of the unit vector **m** (see Figure 5a) along the monomer unit in the main chain, parallel and perpendicular to the direction of the deformation. 8×80 system, $\dot{\gamma} = 0.005$ Å/ps. In all cases the anisotropy of both global and local orientation is clearly seen beyond the yield point.

tion of the monomers in the backbone: the average scalar product of the vectors **n** and **m** is very close to unity (0.97−0.98) over the whole range of deformations. Note that both the global orientation of the chains and their local orientation are weakly temperature dependent.

4. Simulated Local Translational Mobility

The effect of the uniaxial deformation on the segmental translational mobility has been studied by measuring the mean-square translational displacement $\langle \Delta r^2(t)_{\text{par,per}} \rangle$ (MSTD) of individual beads both in the backbone and in the side phenyl groups, parallel and perpendicular to the direction of the deformation. Figure 7a,c shows the results for the side groups MSTD only; qualitatively, the same picture was observed for the segments in the backbone. Ensemble averaging has been performed for all chains and individual side groups. In the elastic regime (deformation less than 3% and time less than 300 ps, with $\dot{\gamma} = 0.005$ Å/ps) the motion of a chain bead is becoming more and more restricted with decreasing temperature: the onset of the Rouse diffusion with the characteristic power $\alpha \sim 0.5$ is preceded by some plateau. As already discussed in

our previous publications,[16,17] this plateau is connected with the cage effect, whereby very restricted local motions occur in the cage formed by surrounding monomers. Qualitatively, the same picture is valid for the motion of the individual beads of the backbone.

The translational behavior changes drastically (as compared to the isotropic case) after the yield point. For time $t \geq 500$ ps the mean-square parallel translational displacement increases almost quadratically with time, as obviously the individual beads on average move convectively in the direction of the deformation. At the same time the mean-square perpendicular displacements increase almost linearly with time.

To subtract the trivial effect of the convective translational motion due to the uniaxial extension and to reveal the effect of the deformation on the fluctuating Brownian contribution to the translational mobility, the following procedure is implemented. First, for each bead of each chain in the polymer sample the average-in-time (for a time interval of 40 ps) position is calculated. The length of the time interval is chosen in order to have, from one side, almost constant average convective mean-square displacement over this time and, from the other side, almost zero contribution of the Brownian term. The MSTD of such averaged positions is then calculated and is obviously treated as a regular convective MSTD. Subtracting this part from the total MSTD gives a mean-square displacement due to the stochastic Brownian motion under the influence of the external deformation. Such "corrected" displacements are shown in Figure 7b,d, together with the MSTD for the side groups in the isotropic sample at the same temperatures. It is clearly seen that the deformation does not influence significantly the translational mobility below the yield point (up to strains less than 3%) in both directions. Dramatic changes occur in the postyield behavior: for the MSTD in the direction of the deformation the onset of the "cage escape" starts significantly earlier as compared to the isotropic case (Figure 7b). At the same time the MSTD in the perpendicular direction remains almost unaffected by the deformation (Figure 7d). We conclude here that the uniaxial mechanical deformation leads to an anisotropy of the local translational mobility, with an acceleration of the parallel diffusion by more than an order of magnitude.

The final parts of the MSTD curves in the elastic regime in Figure 7b are fitted with the power law

$$\langle \Delta r^2(t)_{\text{par}} \rangle \sim (t/\tau_{\text{par}})^{1/2} \qquad (6)$$

where τ_{par} is a characteristic time for the translational diffusion in the direction of the deformation in the regime of the Rouse diffusion. Recently, we have shown that in the absence of the deformation this time is connected to the characteristic time of the α-relaxation; its temperature dependence is well described by the mode-coupling theory at $T > T_g$ and by a simple activation law below T_g.[17] The absolute values of the translational diffusion times τ_{par} under deformation are very close to each other both for the main-chain and side beads and significantly smaller than in the absence of the deformation (Figure 8). We conclude here that the onset of the "cage release" due to the activated "hopping" process starts at earlier times under the influence of the uniaxial deformation. The temperature dependence of the translational diffusion times τ_{par} is also described by a simple activation law, with the same activation
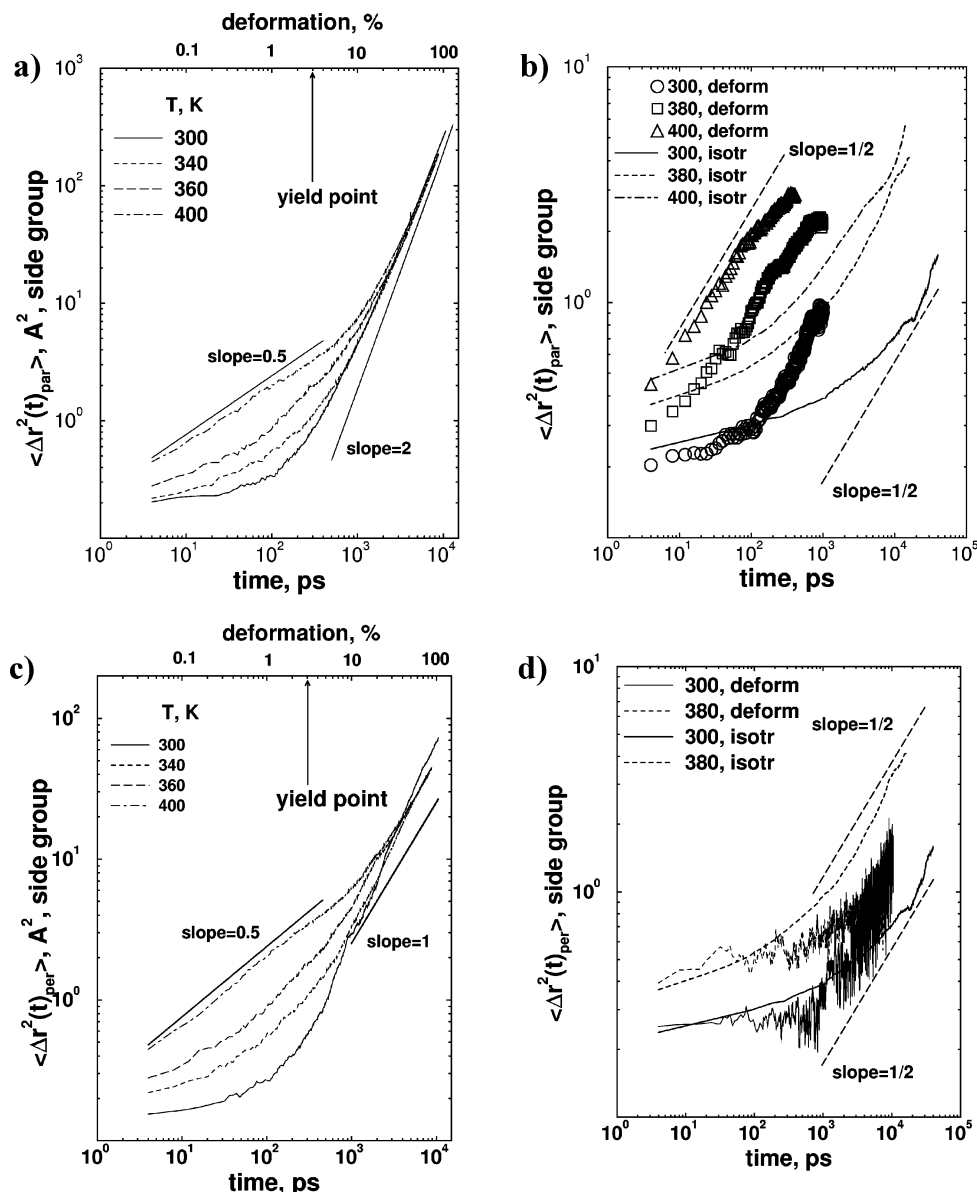
Figure 7. Mean-square translational displacement (MSTD) for the side group in the direction of the deformation (a) and in the perpendicular direction (c). Beyond the yield point $\langle\Delta r^2(t)_{par}\rangle \sim t^2$ and $\langle\Delta r^2(t)_{per}\rangle \sim t$. The fluctuating Brownian contribution to the parallel (b) and perpendicular (d) MSTD is shown together with the corresponding dependencies in the absence of the deformation. The slope of the final parts of the curves in the elastic regime ($t < 300$ ps) is close to 0.5 (Rouse diffusion), but the onset of the Rouse regime in the direction of the deformation starts earlier as compared to the isotropic case. The perpendicular diffusion is weakly changed by the deformation. 8×80 system, $\dot\gamma = 0.005$ Å/ps.

energy $E_a \sim 30$ kJ/mol as in the isotropic case (Figure 8).

5. Simulated Quenched vs Annealed Behavior

Quenching of the 4×160 PS melt was performed from $T = 600$ K to $T = 260$ K during the time of about 2 ps, with an effective cooling rate more than 3 orders of magnitude faster than the regular cooling rate implemented in the present study. Here we would like to report only very preliminary results of the comparison of the mechanical behavior of these computationally quenched and annealed samples.

At $T = 260$ K the preyield stress−strain behavior for the annealed and quenched samples is quite different (Figure 9a). The quenched sample shows a smaller Young modulus at deformations $\gamma_L < 3\%$, and the yield peak is almost erased, as compared to the annealed sample. At the same time the postyield behavior is quite

similar. This characteristic picture is in qualitative agreement with the experimentally observed mechanical rejuvenation phenomenon,[2] or erasure of the aging history, by plastic deformation. Such a rejuvenation has been simulated recently by Utz, Debenedetti, and Stillinger[25] for a binary low-molecular-weight Lennard-Jones mixture. Utz et al.[25] concluded that such a rejuvenation occurs when the system is expelled from the vicinity of deep minima in the potential energy surface.

Some indirect insight into the distribution of the free volume in the samples with different thermal history can be obtained from the dependence of the density on the deformation (Figure 9b). For the annealed sample there is a dilation effect as the tension is applied and the density decreases until the yield point. For the quenched sample densification under the deformation occurs, which could be connected with a relaxation of
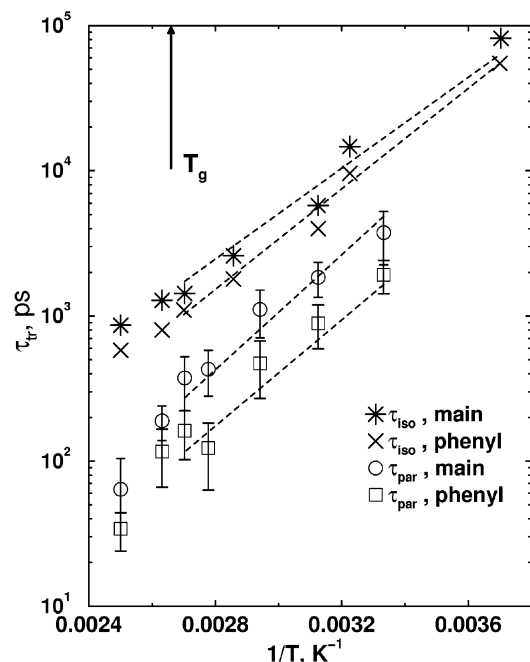
Figure 8. Temperature dependence of the characteristic time of the translational mobility in the isotropic case and under deformation. All dependencies are well described by a simple activation law for both the backbone and phenyl rings diffusion, with the same activation energy $E_a \sim 30$ kJ/mol, in both the isotropic and deformed cases.

the free volume forced by the deformation. For both samples the density converges to the same value just before the yield point.

6. Conclusions

MD computer simulations of uniaxial mechanical deformation have been performed for a chemically realistic model of an atactic PS in the glassy state. Both the linear elastic and the postyield regime of deformation (up to 100% strain) have been simulated. The values of the Poisson ratio and the Young modulus calculated from the initial parts of the stress–strain curves are in a good agreement with the experimental data. The temperature dependence of the yield peak is well described by the Eyring theory (eq 4) with the value $v \sim 360$ Å^3 for the activation volume. This value is smaller than that reported in the literature. The difference could be connected to rather fast sub-T_g relaxation processes (γ, δ) contributing to the stress at the inevitably very high simulated deformation rate of the present study. In the postyield behavior the initial strain-softening, followed by the strain-hardening, is well reproduced. The quenching of the PS melt performed with an effective cooling rate of 170 K/ps (as compared to the rate of 0.05 K/ps for regular simulation runs) leads to striking differences in the mechanical properties in the preyield regime. First of all, the quenched sample shows a smaller Young modulus, and second, the yield peak is almost erased, as compared to the "computationally" annealed sample. The postyield behavior is similar for both samples. This result supports the experimentally observed picture of the erasure of the aging history by plastic deformation.[2] The strain-hardening modulus is calculated from the slope of the stress–strain curves at large strains and is equal to G_R = 15 MPa at T = 260 K, even in quantitative agreement with existing experiments.[1]
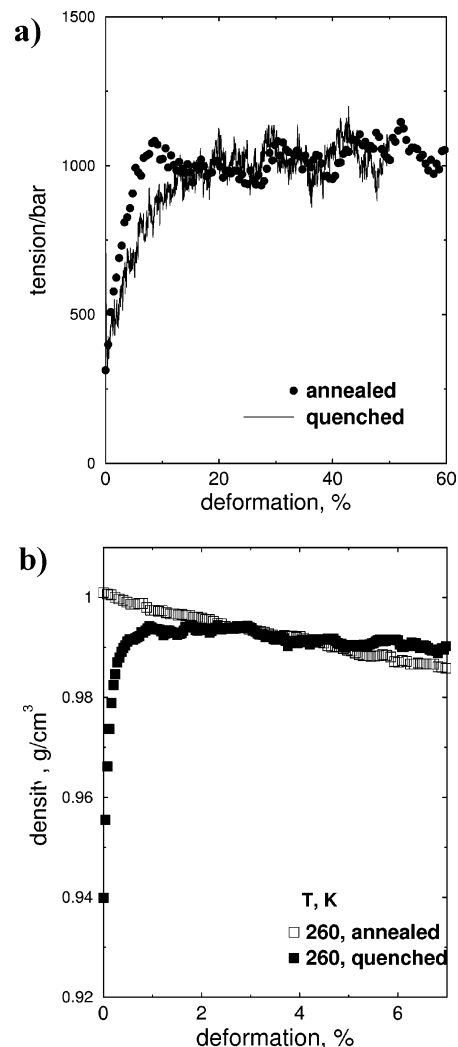

Figure 9. (a) Stress–strain dependence and (b) deformation dependence of the density for the annealed and quenched 4 × 160 samples at T = 260 K. In the stress–strain dependence for the quenched PS the maximum is clearly absent. The initial density for the quenched sample is significantly smaller as compared to the annealed one. The postyield behavior is very similar for both samples.

The uniaxial deformation of the PS sample leads to global orientation of the individual chains in the direction of the deformation. The onset of this orientation starts just after the yield point. The global orientation of the chains takes place together with a local ordering: the monomers in the backbone and the side-group vectors are oriented in the direction of the deformation and perpendicular to it, respectively. At the same time, the planes of the individual phenyl rings are oriented perpendicular to the direction of the deformation.

The orientation of the polymer segments is accompanied by an increase in the anisotropy of the local translational mobility. The fluctuating Brownian part of the mean-square translational displacements of the individual monomers, parallel to the direction of the deformation, increases strongly with percentage deformation. At the same time the transversal projections are weakly influenced by the uniaxial stretching and remain almost the same as the translational displacements in the isotropic sample at the same fixed temperature. Such an increase of the local mobility under the influence of uniaxial mechanical deformation is in qualitative agreement with the results of the recently

reported MD simulations of Capaldi et al.[12] for a model glassy amorphous polyethylene, where the increase in the dihedral angle transition rate under the influence of deformation has been observed. The direct simulation of the isomerization kinetics as well as other local reorientational dynamic properties of the atactic PS glass will be the subject of our future investigation.

References and Notes

(1) van Melick, H. G. H.; Govaert, L. E.; Meijer, H. E. H. *Polymer* **2003**, *44*, 2493.
(2) van Melick, H. G. H.; Govaert, L. E.; Raas, B.; Nauta, W. J.; Meijer, H. E. H. *Polymer* **2003**, *44*, 1171.
(3) Govaert, L. E.; van Melick, H. G. H.; Meijer, H. E. H. *Polymer* **2001**, *42*, 1271.
(4) Kramer, E. J.; Berger, L. L. In *Fundamental Processes of Craze Growth and Fracture*; Kausch, H. H., Ed.; *Adv. Polym. Sci.* **1990**, *91/92*, 1.
(5) Smit, R. J. M.; Brekelmans, W. A. M.; Meijer, H. E. H. *Comput. Methods Appl. Mech. Eng.* **1998**, *155*, 181.
(6) (a) See e.g.: Brule, B.; Halary, J. L.; Monnerie, L. *Proceedings of the 11th International Conference on Deformation, Yield and Fracture of Polymers,* Cambridge, UK, 2000; p 115. (b) Yee, A.; Liu, J.; Li, X. Reference 6a, p 137.
(7) Jérôme, B. *J. Phys.: Condens. Matter* **1999**, *11*, A189.
(8) Brown, D.; Clarke, J. H. R. *Macromolecules* **1991**, *24*, 2075.
(9) Hölzl, T.; Mesner, C.; Wittkop, M.; Kreitmeier, S.; Kain, S.; Göritz, D. *Comput. Theor. Polym. Sci.* **1999**, *9*, 99.
(10) Chui, C.; Boyce, M. C. *Macromolecules* **1999**, *32*, 3795.
(11) Loo, L. S.; Cohen, R. E.; Gleason, K. K. *Science* **2000**, *288*, 116.
(12) Capaldi, F. M.; Boyce, M. C.; Rutledge, G. C. *Phys. Rev. Lett.* **2002**, *89*, 175505.
(13) Neelov, I. M.; Darinskii, A. A.; Clarke, J. *Vysokomol. Soedin.* (*Polym. Sci. USSR*) **1996**, *38*, 1373.
(14) Zhou, J.; Nicholson, T. M.; Davies, G. R.; Ward, I. M. *Comput. Theor. Polym. Sci.* **2000**, *10*, 43.
(15) Ogura, I.; Yamamoto, T. *Polymer* **1995**, *36*, 1375.
(16) Lyulin, A. V.; Michels, M. A. J. *Macromolecules* **2002**, *35*, 1463.
(17) Lyulin, A. V.; Balabaev, N. K.; Michels, M. A. J. *Macromolecules* **2002**, *35*, 9595. Lyulin, A. V.; Michels, M. A. J. *Comput. Phys. Commun.* **2002**, *147*, 298. Lyulin, A. V.; de Groot, J. J.; Michels, M. A. J. *Macromol. Symp.* **2003**, *191*, 167. Lyulin, A. V.; Balabaev, N. K.; Michels, M. A. J. *Macromolecules* **2003**, *36*, 8574.
(18) Allen, M. P.; Tildesley, D. J. *Computer Simulation of Liquids*; Clarendon Press: Oxford, 1987.
(19) Berendsen, H. J. C.; Postma, J. P. M.; van Gunsteren, W. F.; DiNola, A.; Haak, J. R. *J. Chem. Phys.* **1984**, *81*, 3684.
(20) Lemak, A. S.; Balabaev, N. K. *J. Comput. Chem.* **1996**, *17*, 1685.
(21) Baljon, A. R. C.; Robbins, M. O. *Science* **1996**, *271*, 482.
(22) Ward, I. M.; Hadley, D. W. *An Introduction to the Mechanical Properties of Solid Polymers*; John Wiley & Sons: Chichester, 1993.
(23) Govaert, L. E.; de Vries, P. J.; Fennis, P. J.; Nijenhuis, W. F.; Keustermans, J. P. *Polymer* **2002**, *41*, 1959.
(24) Dona, C.-L. *Large Strain Compressive Behaviour of Polystyrene*, MT 02.04 Internal Report, URL: www.mate.tue.nl/mate/showabstract.php/1869, Technische Universiteit Eindhoven, 2002.
(25) Utz, M.; Debenedetti, P. G.; Stillinger, F. H. *Phys. Rev. Lett.* **2000**, *84*, 1471.